

Article

A Double Emulsion-Based, Plastic-Glass Hybrid Microfluidic Platform for Protein Crystallization

Deyong Zhu, Xiaohu Zhou and Bo Zheng *

Received: 17 August 2015 ; Accepted: 22 October 2015 ; Published: 28 October 2015

Academic Editors: Andrew deMello and Xavier Casadevall i Solvas

Department of Chemistry, The Chinese University of Hong Kong, Shatin, Hong Kong, China;
dyzhu@link.cuhk.edu.hk (D.Z.); xhzhou@cuhk.edu.hk (X.Z.)

* Correspondence: bozheng@cuhk.edu.hk; Tel.: +852-39436261; Fax: +852-26035057

Abstract: This paper reports the design and construction of a plastic-glass hybrid microfluidic platform for performing protein crystallization trials in nanoliter double emulsions. The double emulsion-based protein crystallization trials were implemented with both the vapor-diffusion method and microbatch method by controlling the diffusion of water between the inner and outer phases and by eliminating water evaporation. Double emulsions, whose inner and outer environments can be easily adjusted, can provide ideal conditions to explore protein crystallization with the advantages of a convection-free environment and a homogeneous interface. The property of the water-oil interface was demonstrated to be a critical factor for nucleation, and appropriate surfactants should be chosen to prevent protein adsorption at the interface. The results from the volume effect study showed a trend of fewer crystals and longer incubation time when the protein solution volume became smaller, suggesting that the nucleation in protein crystallization process can be controlled by changing the volume of protein solutions. Finally, sparse matrix screening was achieved using the double emulsion-based microbatch method. The double emulsion-based approach for protein crystallization is a promising tool for enhancing the crystal quality by controlling the nucleation process.

Keywords: microfluidic platform; double emulsion; microreactor; protein crystallization; surface effect; volume effect; screening

1. Introduction

The atomic structure of protein molecules is important both for understanding the architectures and functions of living matter and for providing essential knowledge to the pharmaceutical industry, such as new drug discovery and medical therapy [1–3]. There have been several techniques developed for determining the three-dimensional protein structures in laboratories, including X-ray crystallography [4–7], nuclear magnetic resonance spectroscopy (NMR) [8] and cryo-electron microscopy [9,10]. To date, about 90% of the protein structures in the Protein Data Bank (PDB) have been determined using X-ray crystallography [11]. A prerequisite for X-ray crystallography is to produce high-quality protein crystals, which remains one of the bottlenecks in this endeavor [12]. Proteins crystallize in a narrow region of the crystallization phase diagram where nucleation and crystal growth, but not precipitation, occur. The phase diagram is multidimensional and complex, and unfortunately, there are neither comprehensive theories nor a good base of fundamental data to guide our efforts in protein crystallization yet.

Due to the reasons mentioned above, protein crystallization depends generally on trial and error practice up to now. To identify the possible hits and to optimize the conditions for crystallization, large-scale screening in which variable solution ratios of a protein sample with hundreds or even

thousands of precipitants and additives needs to be operated, which may consume a large amount of samples, time and labor. In recent years, great efforts have been made to minimize the volume of each crystallization trial with the development of robotic dispensers [13,14] and microfluidic chips [15,16]. The robotic systems are able to dispense and mix protein and precipitant solutions in microwells or microchambers with nanoliter volumes, and hundreds of thousands of trials can be performed per day. However, the equipment is usually too expensive for most individual laboratories. Alternatively, microfluidic techniques emerge with attractive features in manipulating small volumes (picoliter to nanoliter) of reagents by a relatively simple and economic way [17,18]. Miniaturization through microfluidics can be used to crystallize proteins and provide unique experimental conditions that are either difficult or impossible with macroscopic tools. Different kinds of microfluidic systems, including valve-based systems [19,20], droplets-based systems [21–23] and microwell-based systems [24–28], have been developed to implement the conventional protein crystallization methods of vapor diffusion, microbatch, dialysis and free interface diffusion [1,16].

Emulsions are dispersions of two immiscible fluids, such as water and oil. Multiple emulsions are more complex mixtures as nested groups of several droplets, or “emulsions in emulsions” [29]. Typical examples of multiple emulsions are double emulsions in the form of water-in-oil-in-water (W/O/W) or oil-in-water-in-oil (O/W/O). Double emulsions are attractive systems due to the distinctive and highly hierarchized structures and have a variety of applications, both in industry, such as pharmaceuticals [30], food processing [31] and cosmetics [32], and in the laboratory as “smart microreactors” in which samples are confined and manipulated in small volumes for preceding reactions or delivery, such as quantitative flow cytometric analysis [33], *in vitro* transcription/translation [34] and synthesis of organic molecules and nanoparticles [35]. Emulsion-based approaches for protein crystallization were established to be a promising tool for reducing unwanted heterogeneous nucleation and gaining the chance to obtain one crystal in one droplet [36,37]. The contact between the crystallizing reagents and the wall of supporting containers is one of the factors that induces unwanted heterogeneous nucleation, which is detrimental to X-ray diffraction analysis for protein crystals. To eliminate the contact, Chayen *et al.* [36] developed a “containerless” crystallization technique by suspending a droplet of crystallizing reagents between two immiscible kinds of oils, one of which has a higher density than water and the other one lower, to make the droplet float at the interface. Compared to those protein crystallization trials performed in single emulsions, double emulsions can provide ideal conditions to explore protein crystallization for the advantages of a convection-free environment and a homogeneous interface. An oil shell in double emulsions can separate the crystallizing reagents from the container walls to implement the containerless method. Moreover, a semi-permeable oil shell can provide more controls of the aqueous environment, such as concentration. However, emulsions, especially double emulsions, are thermodynamically unstable systems, which limits their application in long-term experiments, including protein crystallization.

In this work, we developed a new plastic-glass hybrid microfluidic platform for producing and stabilizing nanoliter-scale double emulsions and demonstrated the application of double emulsions for protein crystallization. The traditional vapor diffusion method and microbatch method were both implemented on the present platform. In the traditional way, the vapor diffusion method [38,39] (Figure S1a) is performed by a drop of unsaturated protein and precipitant solution sitting or hanging over a reservoir solution containing relatively concentrated precipitant solution. By equilibration of water vapor from the droplet to the reservoir solution, the protein concentration in the droplet increases, and nucleation starts, followed by crystal growth. The microbatch method [40,41] (Figure S1b) is a miniaturized batch experiment in which protein solution is mixed with precipitant solution and incubates undisturbedly under a low-density inert oil. If the conditions are suitable, the initial mixture will start to form nuclei spontaneously, following the decrease of protein concentration, as crystals begin to grow on the existing nuclei until the line intersects the solubility curve. Our work using double emulsion showed that double emulsion-based approaches yielded

more single crystals per droplet than water-in-oil droplet-based approaches in various volumes. The double emulsion-based approaches provide a simple and economic way for *in situ* serial crystallization in which diffraction data are collected with many small data wedges from a multitude of non-cryocooled and randomly-oriented crystals [42–44].

2. Experimental Section

2.1. Device Fabrication

We produced emulsion droplets using a plastic-glass hybrid microfluidic device fabricated through the co-axial capillary-based scheme (Figure 1) [45]. This hybrid chip was composed of two independent parts: a co-flow junction and a flow-focusing junction. To fabricate the co-flow junction part, glass capillaries, silicone tubing and Teflon tubing were used. As the inner channels, two glass capillaries (Reafine Chromatography Ltd, Hebei, China) with inner diameter (ID) = 100 μm and outer diameter (OD) = 150 μm were cut into a length of about 4 cm and inserted into a piece of 2 cm-long Teflon tubing (Zeus Industrial Products, Raritan, NJ, US) with ID = 300 μm and OD = 600 μm . A piece of silicone tubing (TYGON[®] Tubing, Model S-54-HL, Saint-Gobain Performance Plastics, Akron, OH, USA) with ID = 500 μm was cut with a length of 2 cm, and a hole was punched in the middle through one side of the wall using a needle. The two inner capillaries were threaded through the punched hole, and the Teflon tubing was inserted into the silicone tubing to a depth of 3–5 mm for fixing. The ends of the two inner capillaries were aligned inside the Teflon tubing under a microscope. Ultraviolet (UV) glue was used to seal the punched hole and to fix the two inner capillaries simultaneously. Finally, another three pieces of Teflon tubing were connected to the exposed ends of the two inner capillaries for loading the inner aqueous phases and to the silicone tubing for loading the oil phase, respectively.

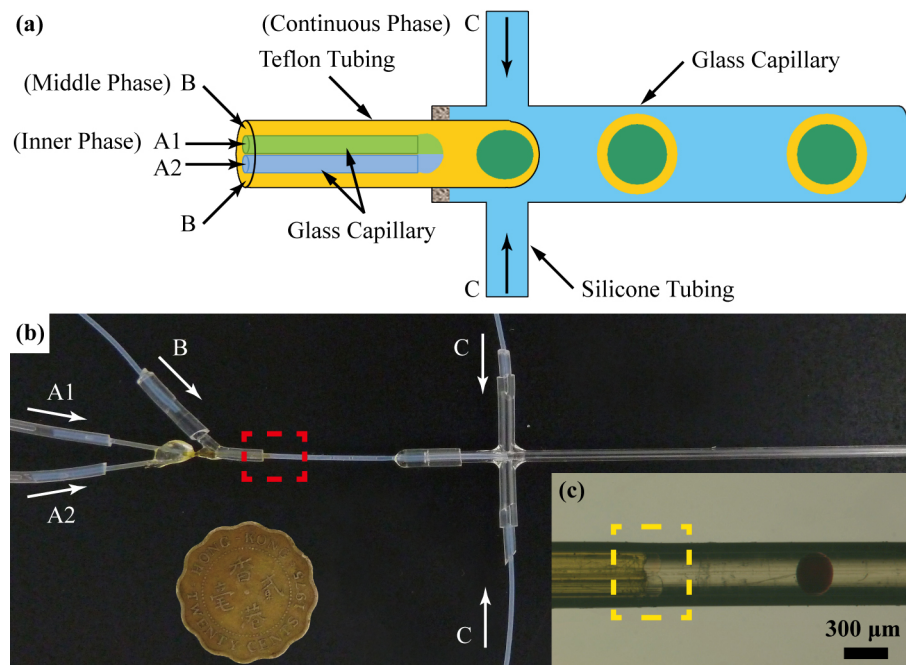


Figure 1. (a) Schematic illustration and (b) photograph of the plastic-glass hybrid microfluidic device with a Hong Kong 20-cent coin; (c) Optical microscope image showing the co-flow junction as highlighted with a red rectangle in (b). The reagent mixing between the two innermost aqueous streams of 0.27 M FeCl_3 and 1 M potassium thiocyanate (KSCN) for the innermost streams A1 and A2, respectively, within the yellow rectangle.

To fabricate the flow-focusing junction, glass capillary and silicone tubing were used. Two small holes were drilled through a glass capillary with ID = 0.86 mm and OD = 1.5 mm (Sutter Instrument, Novato, CA, USA). A piece of silicone tubing was cut into a length of 3 cm and throughout hole was drilled in the middle with the size smaller than the OD of the glass capillary. Thereafter, the glass capillary was inserted through the holes of the silicone tubing, and the two holes on the capillary were adjusted to face the silicone tubing outlets for loading the continuous phase. UV glue was used to enforce the sealing and fixing.

To assemble the plastic-glass hybrid device, two pieces of silicone tubing were used as the connector of the two parts. The smaller silicone tubing was portable for connecting the Teflon tubing of the first part, while the larger silicone tubing was for connecting the glass capillary of the second part. During all steps, heating the silicone tubing for a few minutes can soften the tubing and make the insertion of Teflon tubing or glass capillaries significantly easier. Moreover, this hybrid microfluidic device needs no surface treatment, as Teflon in the first junction is non-wettable to all of the reagents used in this work and suitable for producing water-in-oil emulsions, while the glass in the second junction is hydrophilic enough for oil-in-water emulsion generation. Besides, replacing or washing each of the two junctions is easy for the purpose of reuse.

2.2. Microfluidic Production of Emulsions

For demonstrating the performance of the plastic-glass hybrid microfluidic device, FeCl₃ (Merck-Schuchardt, Hohenbrunn, Germany) and potassium thiocyanate (KSCN) (International Laboratory, San Francisco, CA, USA) were dissolved in deionized (DI) water at a concentration of 0.27 M and 1 M, respectively. Blue food dye (McCormick & Company, Sparks, MD, USA) solution was diluted 20 times with DI water. The aqueous continuous phase for producing W/O/W double emulsions contained 0.5% (*w/v*) sodium dodecyl sulfate (SDS, Analytical Reagent) as the surfactant. Fluorinated oil FC-40 (3M) was used as the continuous phase for producing water-in-oil (Al's oil)-in-oil (fluorinated oil) (W/O/F) double emulsions. All of the aqueous solutions were filtered by a 0.45-micron filter membrane (DISMIC-3cp, Advantec, Tokyo, Japan) prior to use. Al's oil was prepared by mixing an equal volume ratio of silicone oil (Fluid 5, Brookfield, Middleborough, MA, USA) and paraffin oil (Batch: 10C240521, BDH, VWR, Fontenay-sous-Bois, France) to adjust the permeability of water across the oil shell [46]. Surfactants dissolved in the oil phase were 749 Fluid (Dow Corning, Midland, MA, USA), ABIL EM 90 (Owen, Guangzhou, China) or KF-6038 (Shin-Etsu Chemical Company Ltd, Tokyo, Japan) in different cases. All liquids were loaded into the microfluidic device via Teflon tubing using syringe pumps (Model PHD 2000, Harvard Apparatus, Holliston, MA, USA) to control the flow rates. The pipette tips for collecting and storing double emulsions were purchased from Volac. The emulsions for both on-chip formation and inside storage containers were imaged with a CCD camera (SPOT Insight, Diagnostic Instruments, Sterling Heights, MI, USA) attached to a stereo microscope (MZ 16, Leica, Harvard Apparatus). The size of emulsions was measured using the software SPOT (Diagnostic Instruments, Sterling Heights, MI, USA) after calibration.

2.3. Reagents and Data Analysis for Protein Crystallization

Four model proteins were used for the crystallization experiments: (1) Chicken egg-white lysozyme (Beyotime, Haimen, China) in 50 mM sodium acetate buffer, pH 4.5; (2) Thaumatin (Wako Pure Chemical Industries Ltd, Osaka, Japan) in 0.1 M N-(2-acetamido)-iminodiacetic acid (ADA) buffer, pH 6.5; (3) trypsin (Sigma-Aldrich) in 10 mM calcium chloride, 10 mg/mL benzamidine hydrochloride, 25 mM 4-(2-hydroxyethyl)-1-piperazineethanesulfonic acid (HEPES) buffer, pH 7.0; and (4) horseradish peroxidase (Sigma-Aldrich, St. Louis, MO, USA) in 0.1 M phosphate buffer, pH 7.2. The precipitant solutions were: (1) 7% (*w/v*) sodium chloride in acetic acid-sodium acetate buffer, pH 4.6 for lysozyme; (2) 2.0 M sodium potassium tartrate in 0.1 M HEPES buffer, pH 7.5 for thaumatin; (3) 0.2 M ammonium sulfate and 30% (*v/v*) polyethylene glycol (PEG) 8000 in 0.1 M

sodium cacodylate buffer, pH 6.5 for trypsin; and (4) 0.2 M calcium chloride, 28% (*v/v*) PEG 400, 0.1 M HEPES buffer, pH 7.5 for horseradish peroxidase. Different concentrations of each protein were prepared in the buffer solutions according to the objectives discussed in the following sections. All of the reagents were stored at 4 °C and filtered by a 0.45-micron filter membrane prior to use. The crystallization results for each protein crystallization trial were examined by a polarized light stereomicroscope (MZ 16, Leica, Germany) equipped with a CCD camera (SPOT Insight, Diagnostic Instruments, Sterling Heights, MI, USA). The fluorescent images showing the observation of protein adsorption at liquid-liquid interfaces were taken by a laser scanning confocal microscope (C1Si, Nikon, Tokyo, Japan).

3. Results and Discussion

3.1. Performance of the Hybrid Microfluidic Device

Single and double emulsions with different sizes were generated by changing the flow rates using the plastic-glass hybrid microfluidic device. The optical images and diameter distribution analysis of the collected single and double emulsions in Figure 2a–d showed a high level of monodispersity. Even higher-order emulsions can also be produced by changing the flow rates of the inner and middle phases using this hybrid device (Figure 2e). Figure 2f showed the variation in the mean volume of the inner solutions as a function of the flow rate ratio between the sum of the two inner fluid streams and the oil phase. The typical volume of the innermost solution ranged from about 10–120 nanoliter (nL) using the presented plastic-glass hybrid microfluidic device. The narrow error bar indicated a high repeatability of the generated emulsions, suggesting the potential to perform paralleled experiments within these emulsion droplets with identical volume.

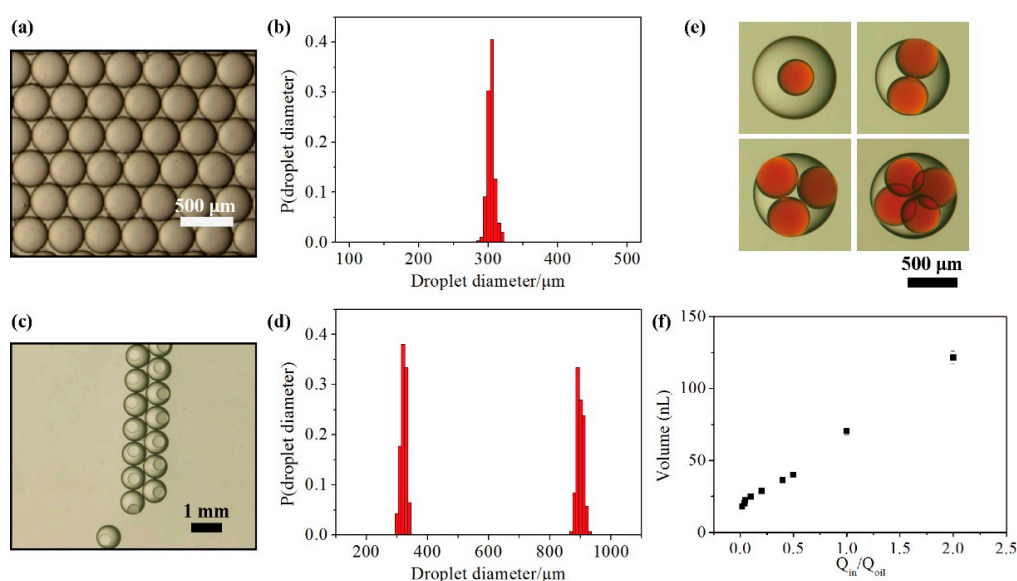


Figure 2. (a,c) Optical microscopic images showing single and double emulsions, respectively; (b,d) Performance of the plastic-glass hybrid microfluidic device by analyzing the diameter distribution of the collected single emulsions (b) and double emulsions (d); (e) Optical microscopic images showing multiple emulsions containing single, double, triple and quadruple core droplets, respectively; (f) Volume variation of the innermost solutions by applying different flow rate ratios of the inner aqueous phase and the middle oil phase.

3.2. Stability and Mass Transport of Double Emulsions

There are several factors that affect the stability of emulsions, such as preparation methods, compound formulation, storage conditions, and so forth [47]. Here, we focused on storing double

emulsions under different environments with the results shown in Figure 3a. The produced double emulsions were collected in: Petri dishes, pipette tips (Figure S2a) or Petri dishes with a thin Teflon membrane to cover the liquid surface (Figure S2b), for subsequent characterization at different time intervals. For double emulsions stored in Petri dishes, a common storage container in the laboratory, nearly all of these double emulsions broke down within four hours (Figure 3a). Several common scenarios were observed during the breakdown of these emulsions: (i) Most of the double emulsions lost their core droplets to form oil-in-water single emulsions at the very beginning stage, usually within one hour; (ii) Some of the double emulsions fused to form larger multiple emulsions that contained several core droplets; (iii) The core aqueous droplets encapsulated in the newly-formed multiple emulsions further fused to grow into even larger emulsions and finally broke down with separated phases after about several days.

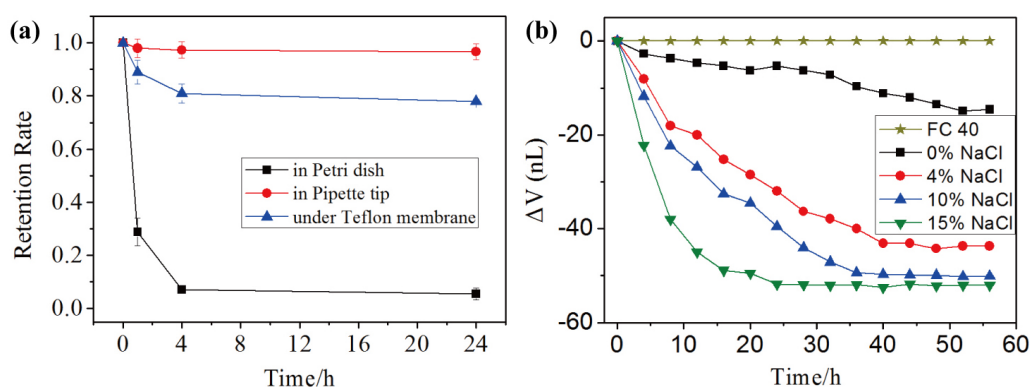


Figure 3. (a) Plot of the retention rate of double emulsions produced by the plastic-glass hybrid microfluidic device under different storage conditions as a function of time; (b) Plot of the change in the volume of the core droplets inside double emulsions (ΔV) against different concentrations of NaCl and FC 40 oil in the continuous phase as a function of time.

On the other hand, the retention rate of double emulsions was found to increase significantly when stored in the pipette tips or under the Teflon membranes compared to that in Petri dishes merely (Figure 3a). We owed the great improvement to three reasons: isolation of the double emulsions from the air-liquid interface, the low dispersion density and the reduction of external disturbance. Because all of the oils used in these experiments have a lower density than that of water, double emulsions would float up and tend to aggregate at the air-liquid surface. Creaming was observed to be a very rapid process in this system due to the relatively large emulsion radius, the large density differences and the low viscosity of the continuous phase. When stored in the pipette tips or under the Teflon membranes, double emulsions were protected from the air-liquid interface, as the adhesive forces between the molecules of two liquid phases at the interface were greater than those of the liquid and air phases. Consequently, the lower surface free energy would help to decrease the breakdown of the double emulsion systems. Meanwhile, the double emulsions were much less likely to aggregate in pipette tips or under Teflon membranes, as the dispersion density of double emulsions could be controlled to be low. Less disturbance would occur during storage because a more closed system was formed in pipette tips or under Teflon membranes.

The water permeability of the oil layer in W/O/W emulsions driven by osmotic pressure gradients between the two aqueous phases has been well addressed by previous studies elsewhere [48–52]. In this study, the mass transport of water across the oil shell of double emulsions was demonstrated using food dye aqueous solution in the core droplets concentrated against the continuous phase containing different concentrations of NaCl solution. Al's oil with 2% (*w/v*) ABIL EM 90 was used as the middle oil phase. Besides the salt NaCl, the continuous phase contained 0.5% (*w/v*) SDS as surfactants additionally. The results in Figure 3b showed that the enrichment rate

increased with larger concentration differences between the inner and outer phases. Similar osmotic gradient can be generated with non-ionic polymers, such as PEGs and dextran, which are widely adopted in biological studies to create osmotic stresses [53]. These results would help to render double emulsions as microreactors with more dynamic control of the reaction process.

3.3. Double Emulsion-Based Approach with the Vapor Diffusion Method

The crystals of the four model proteins were obtained successfully in the W/O/W double emulsions with the vapor diffusion method. The typical appearances of the crystals are shown in Figure 4. In these experiments, the continuous phase was DI water containing 0.5% (*w/v*) SDS and appropriate concentration of PEG 8000, while the middle oil phase was Al's oil with 2% (*w/w*) ABIL EM 90, which played the role of a semipermeable membrane to allow only water molecules to transport into or out of the inner aqueous phase depending on the osmotic gradient. In the beginning, the continuous aqueous phase containing a certain concentration of PEG 8000 provided a higher osmotic pressure compared to the inner aqueous phase with protein solution. The water molecules exit through the oil shell from the inner aqueous phase driven by the osmotic pressure until a balance is reached. Considering the emulsion size, Laplace pressure could be ignored here compared to the osmotic pressure difference. The dehydration of the inner aqueous phase initiated the nucleation followed by the nuclei growth, which was similar to the vapor diffusion process. The osmotic pressure of the continuous aqueous phase was adjusted by changing the PEG 8000 concentration, as shown in Table 1.

Different protein concentrations were tested to evaluate the concentration effect on the protein crystallization process. The probability of successful crystallization trials was evaluated by the ratio between the number of double emulsions that were found to contain crystals inside and the total number of double emulsions initially tested for the trial. As shown in Figure 5, the results suggested that a higher protein concentration increased the success rate of crystallization within the tested concentration range, which meant the presence of more protein molecules increased the nucleation probability. However, the total success rate using this double emulsion-based implementation with the vapor diffusion method was relatively low under the applied crystallization conditions, suggesting that more optimization should be needed, including longer incubation time and finer adjustment of the osmotic pressure difference [54]. On the other hand, for the double emulsions that contain crystals, most emulsion droplets contained a single crystal with a relatively large size, even at the high protein concentration tested in the experiments, which indicated a significant decrease in uncontrolled heterogeneous nucleation compared to that using conventional methods (as shown in Figure S3).

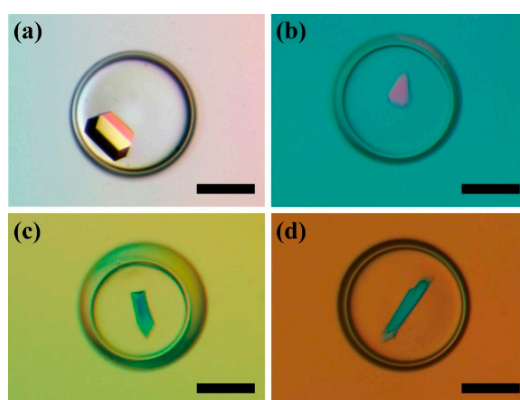


Figure 4. Protein crystallization results using the double emulsion-based approach to implement the vapor diffusion method for: (a) Lysozyme; (b) Thaumatin; (c) Trypsin; (d) Horseradish peroxidase. Scale bars: 300 μm .

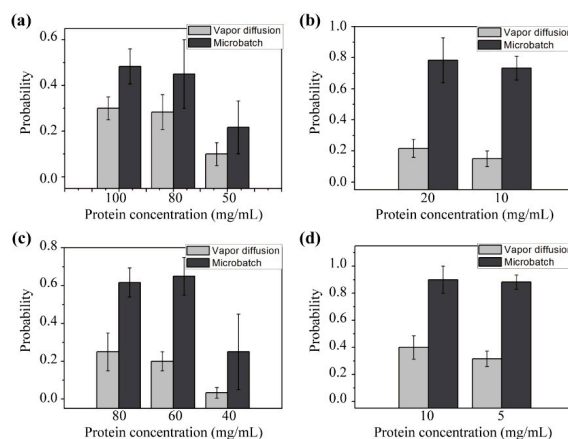


Figure 5. Probability of successful crystallization trials under different protein concentrations using the double emulsion-based approach to implement the vapor diffusion method and microbatch method for: (a) Lysozyme; (b) Thaumatin; (c) Trypsin; (d) Horseradish peroxidase.

Table 1. The applied concentration of PEG 8000 in the continuous phase with different protein solutions.

Protein	Concentration (mg/mL)	Applied Concentration of PEG 8000 (% <i>w/w</i>)
Lysozyme	100/80/50	40
Thaumatin	20/10	40
Trypsin	80/60/40	30
Horseradish peroxidase	10/5	35

3.4. Double Emulsion-Based Approach with the Microbatch Method

The crystals of the four model proteins also grew successfully in the W/O/F double emulsions with microbatch method. The typical appearances of the crystals for the four proteins are shown in Figure 6. In these experiments, the continuous phase was FC-40 fluid, while the middle oil phase was Al’s oil with 2% (*w/w*) ABIL EM 90. FC 40 can serve as an inert sealant to prevent evaporation, as FC-40 is immiscible to either the inner aqueous phase or the oil phase. Consequently, no chemical exchange was expected (Figure 3b) and facilitated the microbatch process.

Different from the double emulsion-based vapor diffusion method, the success rate in this case was much higher and more consistent with the trials using the conventional methods (Figure 5). On the other hand, in both vapor diffusion and microbatch methods, the double emulsions presented single crystals in most droplets, suggesting that the double emulsion-based approaches effectively prevented unwanted heterogeneous nucleation due to the completely homogeneous interface environment.

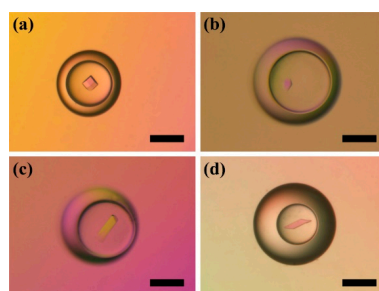


Figure 6. Protein crystallization results using the double emulsion-based approach to implement the microbatch method for: (a) Lysozyme; (b) Thaumatin; (c) Trypsin; (d) Horseradish peroxidase. Scale bars: 300 μm .

3.5. Effect of Protein Adsorption at the Liquid-Liquid Interface on Protein Crystallization

Compared to the experiments operated in batch, double emulsions are more sensitive to interfacial effects because the surface-to-volume ratio increases significantly [55]. Besides the study of proteins, the interface effect has been widely employed to synthesize and assemble many valuable materials, such as inorganic crystals [56], metal nanoparticles [57,58] and composite nanocrystals with integrated and collective functionalities [59,60]. The well-documented phenomenon of adsorption at the interface is expected to have a significant influence on the process of protein crystallization. Meanwhile, proteins themselves show strong interfacial activities in water/oil systems, as protein molecules usually contain both hydrophilic and hydrophobic domains. In general, the promotion of attractive protein-protein interactions can lead to aggregation, which is a critical step in protein crystallization. However, it is still not clear whether the protein adsorption at water/oil interface would either enhance or reduce protein dehydration at the interface to affect the crystallization process in the double emulsions with a completely homogeneous interface [61].

To evaluate the interface effect on protein crystallization, crystallization trials of the model protein lysozyme (100 mg/mL) were performed in plugs, single droplets and double emulsions. For the plugs and single droplets, there was usually direct contact between the protein solutions and the container walls. Surface deformation was obvious, especially in plugs. Contrarily, crystallization reagents were protected from the container wall by the oil shell in the case of double emulsions. The ideal spherical shape of the core droplets in double emulsions could provide a more homogeneous interface environment compared to plugs and single droplets. To further control the interaction between the protein molecules and the interface, two surfactants, 749 Fluid and ABIL EM 90, were added to the oil phase separately. The crystallization outcomes are shown in Figure 7. Both the plugs and single droplets surrounded by the surfactants of either 749 Fluid or ABIL EM 90 could produce crystals, while crystals appeared in the double emulsions only with ABIL EM 90 as the surfactant (Figure 7f), but not with 749 Fluid as the surfactant (Figure 7c).

We believe protein adsorption at the W/O interface was one of the major reasons for the differences in the crystallization results from double emulsions. There were in total three kinds of surfactants used in this study, which differed in the molecular structures and in the interaction with protein molecules. As shown in Figure 8, 749 Fluid, which is a blend of approximately 50% trimethylsiloxysilicate and 50% cyclomethicone (decamethylpenta-cyclosiloxane), showed a strong interaction with protein molecules, while the other two surfactants, ABIL EM 90 and KF-6038, can significantly prevent the interfacial protein adsorption. The molecular structures of 749 Fluid, ABIL EM 90 and KF-6038 are shown in Figure S4. Each of the ABIL EM 90 and KF-6038 molecules contains PEG tails, which have been used as the most common functional group to prevent protein adsorption to interfaces [55,62]. Thereafter, both the vapor diffusion method and the microbatch method were implemented successfully in the double emulsions with the surfactant KF-6038, as shown in Figure S5.

We think the difference in the crystallization results between plugs/single droplets and double emulsions is due to the non-homogeneous interface. Similar to Chayen's containerless method, the oil shell in double emulsions can remain in a spherical shape and separate the crystallizing reagents from the container walls to reduce unwanted heterogeneous nucleation. However, the defects at the water-oil interface in plugs/single droplets may affect the crystallization process by enhancing the nucleation and possibly the number of the nucleation sites [25]. As shown in Figure 7, crystals tended to aggregate and grew in the deformed areas. The deformed and consequently non-homogeneous interface initiated and promoted the nucleation. This phenomenon was also observed in multiple emulsions (Figure S6). The time for the critical nuclei formation usually was a little shorter when there was a deformed surface presented. However, crystals growing under such conditions usually had defects in the structure compared to those growing from a homogeneous interface environment provided by double emulsions.

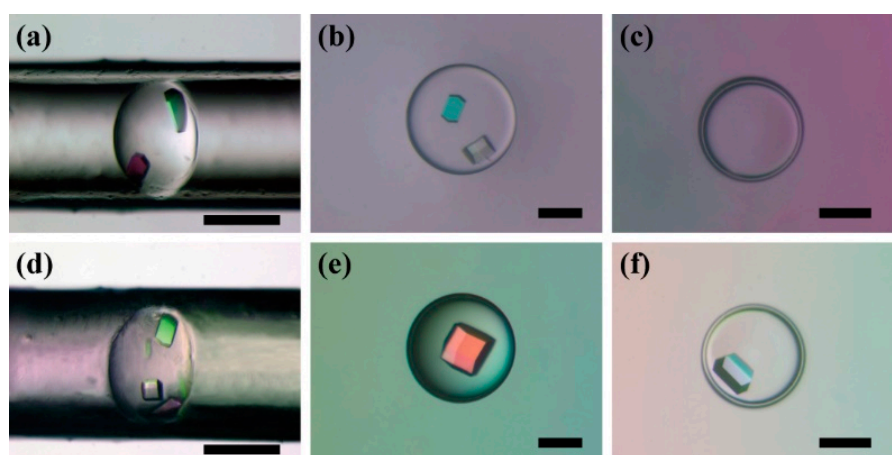


Figure 7. Crystallization results of lysozyme in plugs (a,d), droplets (b,e) and double emulsions (c,f). The oil phases are silicone oil with 3% (*w/w*) 749 Fluid in (a–c) and Al’s oil with 2% (*w/w*) ABIL EM 90 in (d–f). Scale bars: 200 μm.

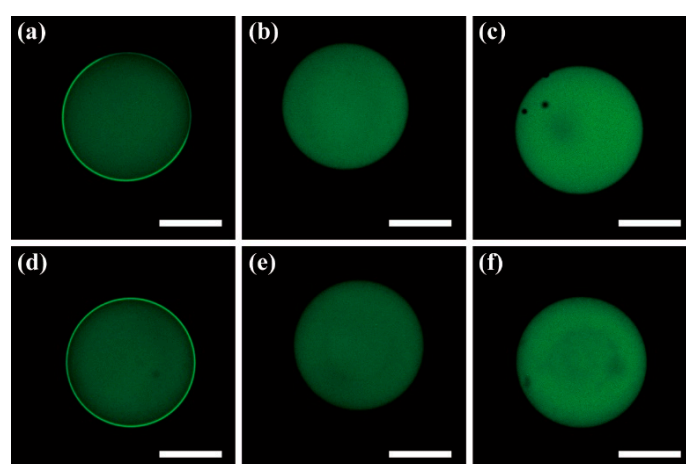


Figure 8. Florescent images showing protein adsorption at the W/O interfaces, which can be either enhanced or prevented. The oil phases in each case are: (a) 749 Fluid; (b) ABIL EM 90; (c) KF-6038; (d) Silicone oil with 3% (*w/w*) 749 Fluid; (e) Al’s oil with 2% (*w/w*) ABIL EM 90; (f) Al’s oil with 1% (*w/w*) KF-6038. The fluorescent protein is eGFP. Scale bars: 500 μm.

3.6. Volume Effect on Protein Crystallization

With the ability to produce identical emulsions in a volume range of nanoliters using the presented microfluidic device, the effect of crystallization reagent volume on the behavior of the protein crystallization process was studied. Two model proteins, thaumatin and horseradish peroxidase, were adopted for crystallization trials using the known crystallization conditions with a series of crystallization reagent volumes ranging from 15–100 nL. To obtain a higher success rate in each microreactor, the emulsion-based microbatch method was used to perform the experiments. The oil phase was paraffin oil with 2% (*w/w*) surfactant ABIL EM 90 to reduce mass transport as much as possible. FC-40 was used as the continuous phase to produce W/O/F double emulsions. The collected plugs, single droplets and double emulsions were incubated and monitored at different time intervals at room temperature (about 21 °C) and high humidity (>95%). Large droplets containing 1 μL crystallization reagent were also performed using the conventional microbatch method as the control experiments.

Differing from the results in large volume droplets, a few empty plugs, single droplets and double emulsions were observed, especially in those with smaller volumes. This result should be owed to the probability of nucleation events decreasing with the reduction in the volume of protein solutions. As shown in Figure 9, more crystals were formed in the plugs and droplets with a larger volume for both thaumatin and horseradish peroxidase. However, the trend was not so obvious for the crystallization trials performed in double emulsions. The probability of one crystal per container became larger in smaller containers in all of the crystallization conditions. Although the success rate was lower compared to the conventional or other emulsion-based methods, it was still worth pointing out that under the tested conditions, double emulsions can help achieve the equilibrium of each container grown with only one crystal, which is the optimal condition for serial crystallography [37,63].

Additionally, the incubation time for protein crystals to appear was also found to relate to the volume of protein solution (Figure 10). In the control experiments, crystals started to form within 4–6 h in the droplets for both tested model proteins. The time consumption could actually change with several folds or even in the order of magnitude among the double emulsion-based methods and the conventional methods. In the nanoliter scale emulsions, a convection-free environment was provided. The growth step, which depends mainly on molecule diffusion, can be regarded as identical for the presented emulsion-based crystallization trials. Therefore, the phenomenon that protein molecules crystallized with a longer time in a smaller solution volume indicated that the probability for nucleation became smaller in reduced volumes. These results agree with the previous studies that the nucleation in the protein crystallization process can be controlled by changing the volume of protein solutions [64–67].

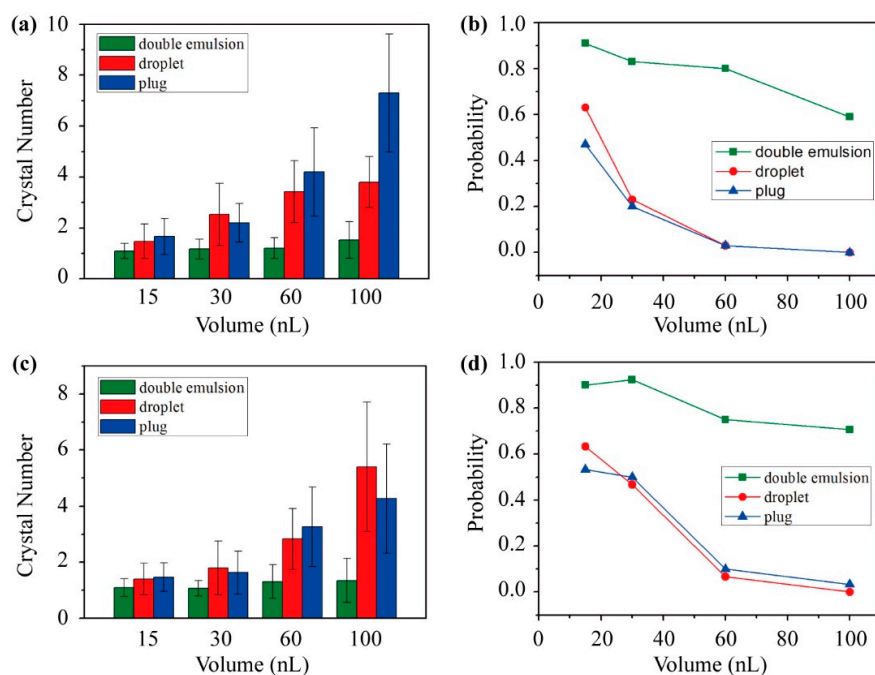


Figure 9. Effects of the protein solution volume in plugs, single droplets and double emulsions on protein crystallization. The number of protein crystals grown in each container with different protein solution volumes for (a) thaumatin and (c) horseradish peroxidase. The relationship between the probability of single crystals grown in the containers and different protein solution volumes for (b) thaumatin and (d) horseradish peroxidase. The model proteins: 20 mg/mL thaumatin and 5 mg/mL horseradish peroxidase.

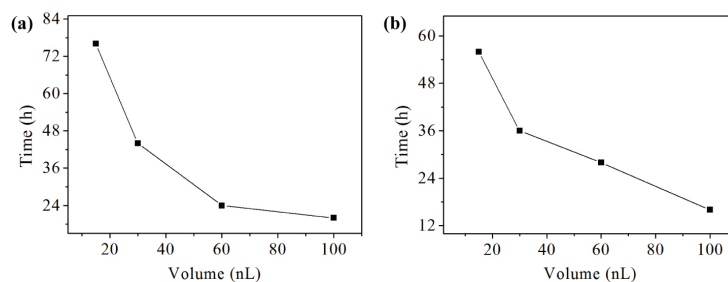


Figure 10. Plot of the incubation time for the protein crystals to appear in double emulsions with different protein solution volumes for (a) thaumatin and (b) horseradish peroxidase. The model proteins: 20 mg/mL thaumatin and 5 mg/mL horseradish peroxidase.

3.7. Double Emulsion-Based Approach for Sparse Matrix Screening

To perform sparse matrix screening by the double emulsion-based approach, the solutions of the crystallization screening kit were firstly preloaded into a piece of Teflon tubing in the form of segments, all of which were separated with fluorocarbon oil and air plugs. The reagent consumption of the protein crystallization screening kit was as small as several microliters for each. To avoid the instability of solution plugs where air bubbles might be trapped unexpectedly in single long Teflon tubing, the screening kit solutions were divided into a few groups and preloaded into several pieces of Teflon tubing within a proper length (<15 cm). The Teflon tubing between the syringe and the plastic-glass hybrid microfluidic device can be replaced with another containing different screening kit solutions to facilitate a high-throughput sparse matrix screening without affecting the performance.

The protein crystallization screening kit used here was Crystal Screen HT™-HR2-130 from Hampton Research (Laguna Niguel, CA, USA), containing 72 screening conditions. The model protein was 20 mg/mL thaumatin, which would be mixed with the screening kit solutions at an equal volume ratio. The double emulsion-based microbatch method was performed for the screening trials with paraffin oil containing 2% (*w/w*) surfactant ABIL EM 90 as the oil phase. As control experiments, the conventional microbatch trials were performed as well with a total of 1 μ L of protein and screening kit solutions at an equal volume ratio. For both the conventional and double emulsion-based microbatch methods, only three of the 72 precipitant conditions resulted in protein crystals, as shown in Figure 11, while all the other 69 results were negative, indicating that the protein crystallization conditions should be similar when using these different methods. A single crystal per container was also obtained for the successful double emulsion-based screening trials.

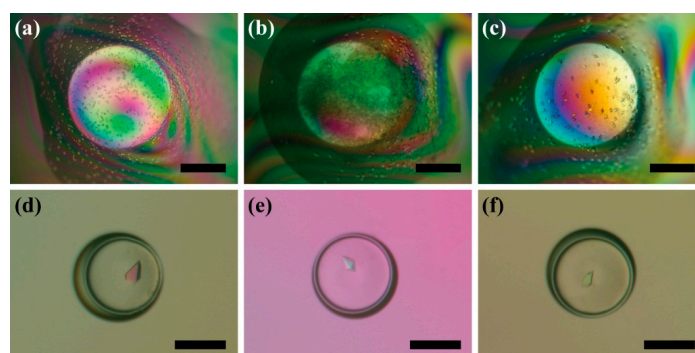


Figure 11. Polarized light photographs showing the screening results for thaumatin under three successful screening conditions: C5 (a,d); D2 (b,e); and F2 (c,f). The upper photographs were obtained by the conventional microbatch method and the lower ones by the double emulsion-based microbatch method. Scale bars: (a–c) 500 μ m, (d–f) 300 μ m.

4. Conclusions

In conclusion, we developed a new plastic-glass hybrid microfluidic platform for producing and storing double emulsions, which can be used as microreactors and applied in the study of protein crystallization. Double emulsions with a high level of monodispersity can be generated using the presented microfluidic device without any surface modification procedures by taking advantage of the wetting property of the composition materials. The lifespans of the double emulsions were prolonged by storing them in confined environments. The isolation of the double emulsions from the air-liquid interface, the protection against external disturbance and the low emulsion dispersion density contributed to the enhanced stability of the double emulsions. The long retention time of the double emulsions provided the opportunity to conduct long-term biological and chemical reactions in these microreactors. To gain more control of the core droplets, the oil shell in double emulsions acted as a semipermeable membrane to cause the core droplets to swell or shrink by changing the composition of the oil phase or the osmotic gradient between the inner and outer aqueous phases.

By using the stable double emulsions as microreactors, four model proteins were crystallized successfully by implementing the classic vapor diffusion method and microbatch method. Surfactants that could prevent protein adsorption at the W/O interface were proven to be a critical factor in the crystallization trials in double emulsions. The convection-free environment and completely homogeneous interface in double emulsions were demonstrated to be able to significantly reduce the unwanted heterogeneous nucleation during the protein crystallization process and to increase the chance to obtain one crystal per container, which is the optimal condition for serial crystallography. The volume effect on protein crystallization was studied using the double emulsion-based microbatch method. Fewer crystals were formed and a longer incubation time was needed with the reduction in protein solution volume within the tested range. The trend suggested that the nucleation in the protein crystallization process can be controlled by changing the volume of protein solutions. We expect the double emulsion-based approach to be able find more applications in basic studies that require fine dynamic controls and that need a large number of parallel or serial chemical and biological reactions.

Supplementary Materials: Supplementary materials can be accessed at: <http://www.mdpi.com/2072-666X/6/11/1446/s1>.

Acknowledgments: This work is supported by the Research Grants Council of Hong Kong (404212).

Author Contributions: D.Z. conducted all of the experiments, interpreted the data and wrote the manuscript. X.Z. assisted with the analysis and mentored the author during the development of the project. B.Z. conceived of the concept of the double emulsion-based approach for protein crystallization, wrote the paper and was the principal investigator of the supporting grants.

Conflicts of Interest: The authors declare no conflict of interest.

References

1. McPherson, A. Introduction to protein crystallization. *Methods* **2004**, *34*, 254–265. [[CrossRef](#)] [[PubMed](#)]
2. Chayen, N.E. Tackling the bottleneck of protein crystallization in the post-genomic era. *Trends Biotechnol.* **2002**, *20*, 98. [[CrossRef](#)]
3. Skolnick, J.; Fetrow, J.S.; Kolinski, A. Structural genomics and its importance for gene function analysis. *Nat. Biotechnol.* **2000**, *18*, 283–287. [[CrossRef](#)] [[PubMed](#)]
4. Deisenhofer, J.; Epp, O.; Miki, K.; Huber, R.; Michel, H. Structure of the protein subunits in the photosynthetic reaction center of *Rhodospseudomonas viridis* at 3 Å resolution. *Nature* **1985**, *318*, 618–624. [[CrossRef](#)] [[PubMed](#)]
5. Doyle, D.A.; Cabral, J.M.; Pfuetzner, R.A.; Kuo, A.L.; Gulbis, J.M.; Cohen, S.L.; Chait, B.T.; MacKinnon, R. The structure of the potassium channel: Molecular basis of K⁺ conduction and selectivity. *Science* **1998**, *280*, 69–77. [[CrossRef](#)] [[PubMed](#)]

6. Palczewski, K.; Kumasaka, T.; Hori, T.; Behnke, C.A.; Motoshima, H.; Fox, B.A.; Le Trong, I.; Teller, D.C.; Okada, T.; Stenkamp, R.E.; Yamamoto, M.; Miyano, M. Crystal structure of rhodopsin: A G protein-coupled receptor. *Science* **2000**, *289*, 739–745. [[CrossRef](#)] [[PubMed](#)]
7. Abola, E.; Kuhn, P.; Earnest, T.; Stevens, R.C. Automation of X-ray crystallography. *Nat. Struct. Biol.* **2000**, *7*, 973–977. [[CrossRef](#)] [[PubMed](#)]
8. Oldfield, E. Chemical-shifts and 3-dimensional protein structures. *J. Biomol. NMR* **1995**, *5*, 217–225. [[PubMed](#)]
9. Adrian, M.; Dubochet, J.; Lepault, J.; McDowell, A.W. Cryo-electron microscopy of viruses. *Nature* **1984**, *308*, 32–36. [[CrossRef](#)] [[PubMed](#)]
10. Kuhlbrandt, W. The resolution revolution. *Science* **2014**, *343*, 1443–1444. [[CrossRef](#)] [[PubMed](#)]
11. Berman, H.M.; Narayanan, B.C.; Di Costanzo, L.; Dutta, S.; Ghosh, S.; Hudson, B.P.; Lawson, C.L.; Peisach, E.; Prlic, A.; Rose, P.W.; et al. Trendspotting in the Protein Data Bank. *Febs Lett.* **2013**, *587*, 1036–1045. [[CrossRef](#)] [[PubMed](#)]
12. Chayen, N.E. Turning protein crystallisation from an art into a science. *Curr. Opin. Struct. Biol.* **2004**, *14*, 577–583. [[CrossRef](#)] [[PubMed](#)]
13. Weselak, M.; Patch, M.G.; Selby, T.L.; Knebel, G.; Stevens, R.C. Robotics for automated crystal formation and analysis. *Methods Enzymol.* **2003**, *368*, 45–76. [[PubMed](#)]
14. Zhu, Y.; Zhu, L.N.; Guo, R.; Cui, H.J.; Ye, S.; Fang, Q. Nanoliter-scale protein crystallization and screening with a microfluidic droplet robot. *Sci. Rep.* **2014**, *4*, 5046. [[CrossRef](#)] [[PubMed](#)]
15. Zheng, B.; Gerdt, C.J.; Ismagilov, R.F. Using nanoliter plugs in microfluidics to facilitate and understand protein crystallization. *Curr. Opin. Struct. Biol.* **2005**, *15*, 548–555. [[CrossRef](#)] [[PubMed](#)]
16. Li, L.; Ismagilov, R.F. Protein crystallization using microfluidic technologies based on valves, droplets and SlipChip. *Annu. Rev. Biophys.* **2010**, *39*, 139–158. [[CrossRef](#)] [[PubMed](#)]
17. Van der Woerd, M.; Ferree, D.; Pusey, M. The promise of macromolecular crystallization in microfluidic chips. *J. Struct. Biol.* **2003**, *142*, 180–187. [[CrossRef](#)]
18. Hansen, C.; Quake, S.R. Microfluidics in structural biology: Smaller, faster... better. *Curr. Opin. Struct. Biol.* **2003**, *13*, 538–544. [[CrossRef](#)] [[PubMed](#)]
19. Hansen, C.L.; Skordalakes, E.; Berger, J.M.; Quake, S.R. A robust and scalable microfluidic metering method that allows protein crystal growth by free interface diffusion. *Proc. Natl. Acad. Sci. USA* **2002**, *99*, 16531–16536. [[CrossRef](#)] [[PubMed](#)]
20. Perry, S.L.; Roberts, G.W.; Tice, J.D.; Gennis, R.B.; Kenis, P.J.A. Microfluidic generation of lipidic mesophases for membrane protein crystallization. *Cryst. Growth Des.* **2009**, *9*, 2566–2569. [[CrossRef](#)] [[PubMed](#)]
21. Zheng, B.; Roach, L.S.; Ismagilov, R.F. Screening of protein crystallization conditions on a microfluidic chip using nanoliter-size droplets. *J. Am. Chem. Soc.* **2003**, *125*, 11170–11171. [[CrossRef](#)] [[PubMed](#)]
22. Zheng, B.; Tice, J.D.; Roach, L.S.; Ismagilov, R.F. A droplet-based, composite PDMS/glass capillary microfluidic system for evaluating protein crystallization conditions by microbatch and vapor-diffusion methods with on-chip X-ray diffraction. *Angew. Chem. Int. Ed.* **2004**, *43*, 2508–2511. [[CrossRef](#)] [[PubMed](#)]
23. Zheng, B.; Ismagilov, R.F. A microfluidic approach for screening submicroliter volumes against multiple reagents by using preformed arrays of nanoliter plugs in a three-phase liquid/liquid/gas flow. *Angew. Chem. Int. Ed.* **2005**, *44*, 2520–2523. [[CrossRef](#)] [[PubMed](#)]
24. Zhou, X.; Lau, L.; Lam, W.W.L.; Au, S.W.N.; Zheng, B. Nanoliter dispensing method by degassed poly(dimethylsiloxane) microchannels and its application in protein crystallization. *Anal. Chem.* **2007**, *79*, 4924–4930. [[CrossRef](#)] [[PubMed](#)]
25. Li, Y.F.; Guo, D.M.; Zheng, B. Rehydratable gel for rapid loading of nanoliter solution and its application in protein crystallization. *RSC Adv.* **2012**, *2*, 4857–4863.
26. Guha, S.; Perry, S.L.; Pawate, A.S.; Kenis, P.J.A. Fabrication of X-ray compatible microfluidic platforms for protein crystallization. *Sens. Actuators B Chem.* **2012**, *174*, 1–9. [[CrossRef](#)] [[PubMed](#)]
27. Selimovic, S.; Gobeaux, F.; Fraden, S. Mapping and manipulating temperature-concentration phase diagrams using microfluidics. *Lab Chip* **2010**, *10*, 1696–1699. [[CrossRef](#)] [[PubMed](#)]
28. Shim, J.U.; Cristobal, G.; Link, D.R.; Thorsen, T.; Jia, Y.W.; Piattelli, K.; Fraden, S. Control and measurement of the phase behavior of aqueous solutions using microfluidics. *J. Am. Chem. Soc.* **2007**, *129*, 8825–8835. [[CrossRef](#)] [[PubMed](#)]

29. Abate, A.R.; Weitz, D.A. High-order multiple emulsions formed in poly(dimethylsiloxane) microfluidics. *Small* **2009**, *5*, 2030–2032. [[CrossRef](#)] [[PubMed](#)]
30. Cournarie, F.; Savelli, M.P.; Rosilio, W.; Bretez, F.; Vauthier, C.; Grossiord, J.L.; Seiller, M. Insulin-loaded W/O/W multiple emulsions: Comparison of the performances of systems prepared with medium-chain-triglycerides and fish oil. *Eur. J. Pharm. Biopharm.* **2004**, *58*, 477–482. [[CrossRef](#)] [[PubMed](#)]
31. Muschiolik, G. Multiple emulsions for food use. *Curr. Opin. Colloid Interface Sci.* **2007**, *12*, 213–220. [[CrossRef](#)]
32. Patravale, V.B.; Mandawgade, S.D. Novel cosmetic delivery systems: An application update. *Int. J. Cosmet. Sci.* **2008**, *30*, 19–33. [[CrossRef](#)] [[PubMed](#)]
33. Yan, J.; Bauer, W.A.C.; Fischlechner, M.; Hollfelder, F.; Kaminski, C.F.; Huck, W.T.S. Monodisperse water-in-oil-in-water (W/O/W) double emulsion droplets as uniform compartments for high-throughput analysis via flow cytometry. *Micromachines* **2013**, *4*, 402–413. [[CrossRef](#)]
34. Wu, N.; Oakeshott, J.G.; Easton, C.J.; Peat, T.S.; Surjadi, R.; Zhu, Y. A double-emulsion microfluidic platform for *in vitro* green fluorescent protein expression. *J. Micromech. Microeng.* **2011**, *21*, 054032. [[CrossRef](#)]
35. Lamprecht, A.; Ubrich, N.; Perez, M.H.; Lehr, C.M.; Hoffman, M.; Maincent, P. Influences of process parameters on nanoparticle preparation performed by a double emulsion pressure homogenization technique. *Int. J. Pharm.* **2000**, *196*, 177–182. [[CrossRef](#)]
36. Chayen, N.E. A novel technique for containerless protein crystallization. *Protein Eng.* **1996**, *9*, 927–929. [[CrossRef](#)] [[PubMed](#)]
37. Akella, S.V.; Mowitz, A.; Heymann, M.; Fraden, S. Emulsion-based technique to measure protein crystal nucleation rates of lysozyme. *Cryst. Growth Design* **2014**, *14*, 4487–4509. [[CrossRef](#)]
38. Hampel, A.; Labanaus, M.; Connors, P.G.; Kirkegar, L.; Rajbhand, U.L.; Sigler, P.B.; Bock, R.M. Single crystals of transfer rna from formylmethionine and phenylalanine transfer rnas. *Science* **1968**, *162*, 1384–1387. [[CrossRef](#)] [[PubMed](#)]
39. McPherson, A. The Growth and Preliminary Investigation of Protein and Nucleic Acid Crystals for X-ray Diffraction Analysis. In *Methods of Biochemical Analysis*; John Wiley & Sons, Inc.: Hoboken, NJ, USA, 1976; pp. 249–345.
40. Chayen, N.E.; Stewart, P.D.S.; Maeder, D.L.; Blow, D.M. An automated-system for microbatch protein crystallization and screening. *J. Appl. Crystallogr.* **1990**, *23*, 297–302. [[CrossRef](#)]
41. Chayen, N.E.; Stewart, P.D.S.; Blow, D.M. Microbatch crystallization under oil—A new technique allowing many small-volume crystallization trials. *J. Cryst. Growth* **1992**, *122*, 176–180. [[CrossRef](#)]
42. Chapman, H.N.; Fromme, P.; Barty, A.; White, T.A.; Kirian, R.A.; Aquila, A.; Hunter, M.S.; Schulz, J.; DePonte, D.P.; Weierstall, U.; *et al.* Femtosecond X-ray protein nanocrystallography. *Nature* **2011**, *470*, 73–77. [[CrossRef](#)] [[PubMed](#)]
43. Gati, C.; Bourenkov, G.; Klinge, M.; Rehders, D.; Stellato, F.; Oberthur, D.; Yefanov, O.; Sommer, B.P.; Mogk, S.; Duzsenko, M.; *et al.* Serial crystallography on *in vivo* grown microcrystals using synchrotron radiation. *IUCr* **2014**, *1*, 87–94. [[CrossRef](#)] [[PubMed](#)]
44. Huang, C.Y.; Olieric, V.; Ma, P.K.; Panepucci, E.; Diederichs, K.; Wang, M.T.; Caffrey, M. In meso *in situ* serial X-ray crystallography of soluble and membrane proteins. *Acta Crystallogr. Sect. D Biol. Crystallogr.* **2015**, *71*, 1238–1256.
45. Utada, A.S.; Lorenceau, E.; Link, D.R.; Kaplan, P.D.; Stone, H.A.; Weitz, D.A. Monodisperse double emulsions generated from a microcapillary device. *Science* **2005**, *308*, 537–541. [[CrossRef](#)] [[PubMed](#)]
46. D'Arcy, A.; Elmore, C.; Stihle, M.; Johnston, J.E. A novel approach to crystallising proteins under oil. *J. Cryst. Growth* **1996**, *168*, 175–180. [[CrossRef](#)]
47. Ficheux, M.F.; Bonakdar, L.; Leal-Calderon, F.; Bibette, J. Some stability criteria for double emulsions. *Langmuir* **1998**, *14*, 2702–2706. [[CrossRef](#)]
48. Matsumoto, S.; Inoue, T.; Kohda, M.; Ikura, K. Water permeability of oil layers in W/O/W emulsions under osmotic pressure gradients. *J. Colloid Interface Sci.* **1980**, *77*, 555–563. [[CrossRef](#)]
49. Colinart, P.; Delepine, S.; Trouve, G.; Renon, H. Water transfer in emulsified liquid membrane processes. *J. Membr. Sci.* **1984**, *20*, 167–187. [[CrossRef](#)]
50. Wen, L.X.; Papadopoulos, K.D. Visualization of water transport in $W_1/O/W_2$ emulsions. *Colloids Surf. A Physicochem. Eng. Asp.* **2000**, *174*, 159–167. [[CrossRef](#)]

51. Wen, L.X.; Papadopoulos, K.D. Effects of surfactants on water transport in $W_1/O/W_2$ emulsions. *Langmuir* **2000**, *16*, 7612–7617. [[CrossRef](#)]
52. Bahtz, J.; Gunes, D.Z.; Hughes, E.; Pokorny, L.; Riesch, F.; Syrbe, A.; Fischer, P.; Windhab, E.J. Decoupling of mass transport mechanisms in the stagewise swelling of multiple emulsions. *Langmuir* **2015**, *31*, 5265–5273. [[CrossRef](#)] [[PubMed](#)]
53. Qian, Z.J.; Song, J.J.; Chaumont, F.; Ye, Q. Differential responses of plasma membrane aquaporins in mediating water transport of cucumber seedlings under osmotic and salt stresses. *Plant Cell Environ.* **2015**, *38*, 461–473.
54. Chayen, N.E.; Saridakis, E. Protein crystallization: From purified protein to diffraction-quality crystal. *Nat. Methods* **2008**, *5*, 147–153. [[CrossRef](#)] [[PubMed](#)]
55. Roach, L.S.; Song, H.; Ismagilov, R.F. Controlling nonspecific protein adsorption in a plug-based microfluidic system by controlling interfacial chemistry using fluorosurfactants. *Anal. Chem.* **2005**, *77*, 785–796. [[CrossRef](#)] [[PubMed](#)]
56. Rao, C.N.R.; Kalyanikutty, K.P. The liquid-liquid interface as a medium to generate nanocrystalline films of inorganic materials. *Acc. Chem. Res.* **2008**, *41*, 489–499. [[CrossRef](#)] [[PubMed](#)]
57. Zhang, L.; Wang, Y.; Tong, L.M.; Xia, Y.A. Synthesis of colloidal metal nanocrystals in droplet reactors: The pros and cons of interfacial adsorption. *Nano Lett.* **2014**, *14*, 4189–4194. [[CrossRef](#)] [[PubMed](#)]
58. Sanyal, M.K.; Agrawal, V.V.; Bera, M.K.; Kalyanikutty, K.P.; Daillant, J.; Blot, C.; Kubowicz, S.; Kononov, O.; Rao, C.N.R. Formation and ordering of gold nanoparticles at the toluene-water interface. *J. Phys. Chem. C* **2008**, *112*, 1739–1743. [[CrossRef](#)]
59. Cheng, L.; Liu, A.P.; Peng, S.; Duan, H.W. Responsive plasmonic assemblies of amphiphilic nanocrystals at oil-water interfaces. *Acs Nano* **2010**, *4*, 6098–6104. [[CrossRef](#)] [[PubMed](#)]
60. Zhang, D.T.; Wu, F.X.; Peng, M.H.; Wang, X.Y.; Xia, D.G.; Guo, G.S. One-step, facile and ultrafast synthesis of phase- and size-controlled Pt-Bi intermetallic nanocatalysts through continuous-flow microfluidics. *J. Am. Chem. Soc.* **2015**, *137*, 6263–6269. [[CrossRef](#)] [[PubMed](#)]
61. Silver, B.R.; Fulop, V.; Unwin, P.R. Protein crystallization at oil/water interfaces. *New J. Chem.* **2011**, *35*, 602–606. [[CrossRef](#)]
62. Zhang, Y.; Ho, Y.P.; Chiu, Y.L.; Chan, H.F.; Chlebina, B.; Schuhmann, T.; You, L.C.; Leong, K.W. A programmable microenvironment for cellular studies via microfluidics-generated double emulsions. *Biomaterials* **2013**, *34*, 4564–4572. [[CrossRef](#)] [[PubMed](#)]
63. Heymann, M.; Ophthalge, A.; Wierman, J.L.; Akella, S.; Szebenyi, D.M.E.; Gruner, S.M.; Fraden, S. Room-temperature serial crystallography using a kinetically optimized microfluidic device for protein crystallization and on-chip X-ray diffraction. *IUCr* **2014**, *1*, 349–360. [[CrossRef](#)] [[PubMed](#)]
64. Kashchiev, D.; Verdoes, D.; van Rosmalen, G.M. Induction time and metastability limit in new phase formation. *J. Cryst. Growth* **1991**, *110*, 373–380. [[CrossRef](#)]
65. Laval, P.; Salmon, J.B.; Joanicot, M. A microfluidic device for investigating crystal nucleation kinetics. *J. Cryst. Growth* **2007**, *303*, 622–628. [[CrossRef](#)]
66. Salmon, J.B.; Leng, J. Microfluidics for kinetic inspection of phase diagrams. *Comptes Rendus Chim.* **2009**, *12*, 258–269. [[CrossRef](#)]
67. Jiang, S.F.; ter Horst, J.H. Crystal nucleation rates from probability distributions of induction times. *Cryst. Growth Des.* **2011**, *11*, 256–261. [[CrossRef](#)]



© 2015 by the authors; licensee MDPI, Basel, Switzerland. This article is an open access article distributed under the terms and conditions of the Creative Commons by Attribution (CC-BY) license (<http://creativecommons.org/licenses/by/4.0/>).